Sputtering kilodalton fragments from polymers

A. Delcorte [a,*], B. Arezki [a], P. Bertrand [a], B.J. Garrison [b]

[a] *PCPM, Université Catholique de Louvain, 1 Croix du Sud, B1348, Louvain-la-Neuve, Belgium*
[b] *Department of Chemistry, The Pennsylvania State University, 152 Davey Lab, University Park, PA 16802, USA*

Abstract

The sputtering of large fragments from polystyrene oligomers (7.5 kDa) is investigated using classical molecular dynamics. Simulation results obtained with the new adaptive AIREBO potential including long-range van der Waals interactions are compared to calculations performed with the short-range Brenner potential functions. The model qualitatively accounts for the experimental mass spectra and kinetic energy distributions of heavy kilodalton fragments. Concerning the mechanisms, the simulations show that there exists a transition from an atomic cascade, where atoms collide much like billiard balls, to a molecular motion regime, where the energy is stored in the rotation and vibration modes of the molecule and the motions become collective. Large chain segments are sputtered during the molecular motion stage of the interaction. © 2002 Elsevier Science B.V. All rights reserved.

1. Introduction

Large chain segments are sputtered from polymer coatings bombarded by keV ions. These fragments can be detected in a secondary ion mass spectrometer (SIMS) and used for analytical purpose, provided that they are extrinsically ionized via metal adducts [1,2]. From the fundamental viewpoint, however, the process by which such fragments are sputtered as a result of the keV particle bombardment lacks experimental or theoretical support.

To gain insights into these mechanisms, we investigate the emission of large fragments sputtered from polystyrene oligomers adsorbed on a silver substrate via a combined molecular dynamics (MD) simulation/SIMS approach. Indeed, classical MD simulations provide a valuable mechanistic information concerning the sputtering processes in many cases involving organic molecules [3]. A pioneering attempt at modeling polymer sputtering via a MD algorithm has also been conducted in the past [4], but without long-range van der Waals forces in the model, which might be too drastic an approximation for organic solids. In this paper, we describe the microscopic aspects of the emission of polymer fragments on the grounds of simulations performed with a recently developed potential (AIREBO [5]) that includes long-range forces. To validate the MD model, the simulation results are compared to experimental data obtained by ToF-SIMS. Using the MD model, we investigate the development of the atomic collision cascade in the organic medium and the vibrational excitations of the molecule which ultimately lead to kilodalton fragment desorption.

---

* Corresponding author. Tel.: +32-10-473582; fax: +32-10-473452.
E-mail address: delcorte@pcpm.ucl.ac.be (A. Delcorte).

2. Method

2.1. Molecular dynamics simulations

The Ar bombardment of a *sec*-butyl terminated polystyrene oligomer comprising 61 styrene repeat units $(C_4H_9[C_8H_8]_{61}H)$ adsorbed on a Ag(1 1 1) surface (Fig. 1) is modeled using MD computer simulations. The silver substrate is approximated by a finite microcrystallite containing 7 layers of 208 Ag atoms. The polystyrene oligomer coil is placed on the Ag{1 1 1} surface and the entire system is relaxed to a minimum energy configuration prior to Ar atom impact. The average density obtained for the polystyrene molecule after relaxation is 1.04 ± 0.1 g/cm^3 (1.05 g/cm^3 for bulk polystyrene [6]).

The MD scheme has been described in extensive detail elsewhere [7,8]. The blend of empirical pairwise and many-body potential energy func-

tions used to represent the forces among the various atoms is described in published papers [9,10], except for the adaptive intermolecular potential, AIREBO, developed by Stuart et al. [5]. This potential, based on the reactive empirical bond-order (REBO) potential developed by Brenner for hydrocarbon molecules [11], also includes nonbonding (van der Waals) interactions.

For the bombardment itself, primary Ar atoms are directed along the surface normal. The impact area (rectangle in Fig. 1) is centered on the polystyrene oligomer. About 160 trajectories were calculated with our PS molecule in the AIREBO potential. For comparison purpose, about 1000 trajectories were also calculated with the same sample using the REBO potential. The CPU time per trajectory using the REBO potential is almost one order of magnitude shorter than it is using the AIREBO potential, which explains the larger number of computed trajectories.

2.2. ToF-SIMS measurements

Samples of *sec*-butyl terminated, deuterated PS oligomers ($M_n = 5300$ Da) are dissolved in toluene with a concentration of 3×10^{-3} M. The samples are prepared as thin films cast on 0.25 cm^2 silver foils (Goodfellow; 99.95+ %purity). Prior to organic sample deposition, the substrates are etched in 30% highest purity grade sulfuric acid (Vel) for 3 min, then rinsed in water of high-performance liquid chromatography grade from a milli-Q system (Millipore) and p.a. grade isopropanol (Vel).

The secondary ion mass analyses and the kinetic energy distribution (KED) measurements are performed in a PHI-EVANS time-of-flight SIMS (TRIFT 1 [12]) using a 15 keV Ga$^+$ beam (FEI 83-2 liquid metal ion source) [13]. To improve the measured intensities, the secondary ions are post-accelerated by a high voltage (7.5 kV) in front of the detector. To obtain energy spectra, the signal corresponding to different energy windows is collected through a 100 µm slit (1.5 eV resolution) located at the crossover following the first electrostatic analyzer of the spectrometer. The energy scan is either performed by changing the sample voltage or the slit position [13].
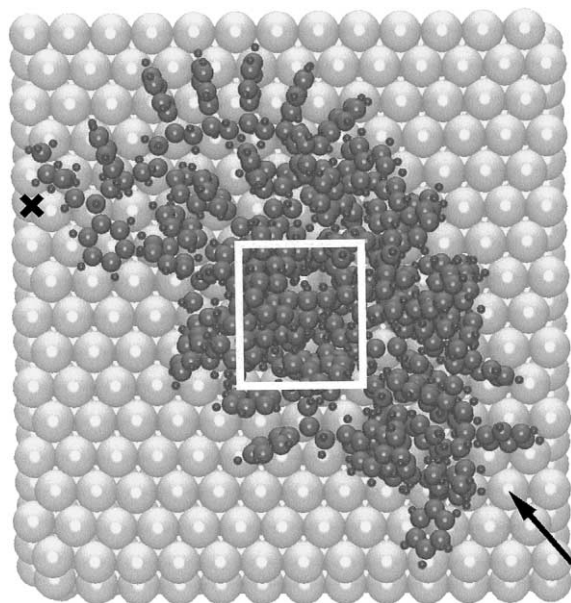
Fig. 1. Top view of the simulation cell. Silver atoms are represented by large light gray spheres, carbon and hydrogen atoms by dark gray spheres. The bombarded area is indicated by a white rectangle. The arrow indicates the position of the viewer in the movie snapshot of Fig. 3. The *sec*-butyl chain end is marked by a cross.

3. Results and discussion

3.1. Nature and kinetic energy of the ejected species

The mass spectra provided by the MD simulations are described in detail elsewhere [14]. Briefly, the main peaks of the mass spectra calculated with either the REBO or the AIREBO potential are: $^{**}C$, $^{**}C_2H_2$, $^*C_3H_2$–C_3H_3, C_4H_3–C_4H_4, C_5H_5, $^*C_6H_5$, C_7H_6–C_7H_7, C_8H_7–C_8H_8 and C_9H_9 (the number of stars mirrors the peak intensity). These are characteristic PS fragments also observed in the experiment. Beyond 1000 Da, the major fragments are of the kind M_n, M_n–CH, where M corresponds to the repeat unit of polystyrene. This means that most of the kilodalton fragments are induced by a single bond-scission in the backbone of the organic molecule. For comparison, four major series of high-mass fragments can be identified in the experimental spectrum [14]: $(M_n + Ag)^+$, $(M_n$–CH $+ Ag)^+$, $(M_n + E + Ag)^+$ and $(M_n + E + CH + Ag)^+$, where E corresponds to the *sec*-butyl endgroup. If one excepts the Ag adduct required for cationization in the experiments, the M_n and M_n–CH type fragments are observed in both the calculated and the experimental spectra. On the other hand, the $M_n + E$ and $M_n + E + CH$ series of fragment are specifics of the experimental mass spectrum. This difference can be easily explained by the arrangement of the polystyrene molecule on the silver surface in the simulation (Fig. 1). Indeed, the *sec*-butyl endgroup (E) is lying on the silver surface, at the rim of the molecule, in the model (cross in Fig. 1). The emission of large fragments buried at the metal–molecule interface is obviously hampered. Accordingly, the analysis of the calculated trajectories shows indeed that the ejected kilodalton chain segments originate from the top of the bombarded molecule. Therefore, our simulations only provide the mass spectrum related to a given configuration of the molecule, whereas the experiment statistically samples all the possible molecular arrangements. Nonetheless, all the kilodalton segments observed in the simulation exist in the experiment, which constitutes a convincing assessment of the model validity.

In order to compare the KEDs of sputtered kilodalton fragments with experimental data, a relatively large number of trajectories must be calculated, mainly because the ejection yield of large polyatomic fragments is very low. Since trajectories computed with the long-range forces (AIREBO) are time consuming, a tractable alternative is to compare experimental energy spectra with calculations performed with the short-range Brenner potential. This approximation is supported by the fact that the nature of the sputtered species and the KEDs of small fragments are similar with the different potentials. In addition, the kilodalton fragments sputtered in the AIREBO scheme also mirror those observed using the Brenner potential [14].

The experimental and calculated distributions of kilodalton fragments are compared in Fig. 2. To obtain a sufficient statistics, the calculated (respectively: experimental) energy spectrum adds up the distributions of all the fragments in the mass range 1000–1500 Da (respectively 1100–1600 Da). Remarkably, the MD model predicts the experimental distribution maximum at 4 eV, but there
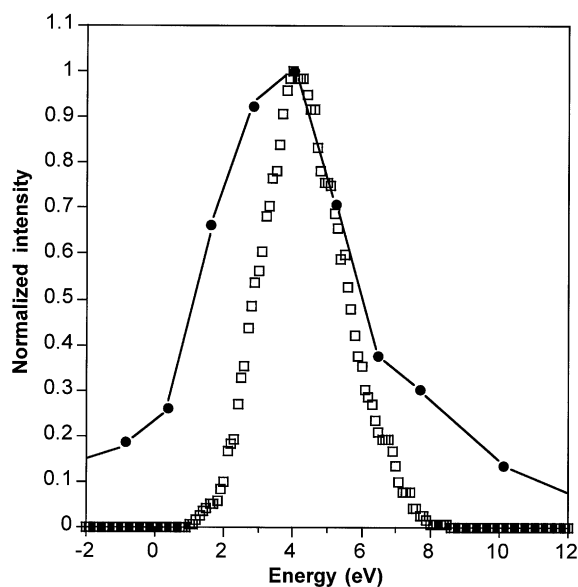
Fig. 2. Calculated KED of fragments (1000 Da$< m <$1500 Da) sputtered from a model PS 61-mer (open squares) and experimental KED of cationized homologue fragments (1100 Da$< m <$1600 Da) (full circles) emitted from a deuterated PS oligomer sample.

are also differences. The intensity corresponding to negative energies, only seen in the experimental spectrum, is an artefact due to unimolecular dissociation reactions in the spectrometer. As discussed in [15], the absence of a high energy tail in the calculated distribution might be due to the higher projectile energy used in the experiment. Finally, the noticeable difference in the range 0–4 eV can be attributed to the cut off induced by the time limit of the simulation (6 ps). Running longer simulations and counting virtually all the ejected fragments would only lead to a distribution broadening towards low kinetic energies. The parallel increase of computer time makes such a choice unreasonable.

The small number of trajectories used for the detailed study of the sputtering mechanisms have been calculated with the AIREBO potential and run up to saturation of the ejected atom number. In that sense, they reflect a more refined model than those considered to calculate the yields and energy distributions in this section.

3.2. Development of the atomic cascade

A typical trajectory has been chosen to illustrate the processes occurring in the sample as it is bombarded by 500 eV Ar atoms. Fig. 3(a) shows the collision tree of that particular trajectory. The collision tree is constituted by the track of atoms in motion in the sample over the first 100 fs of the interaction [15]. It shows the actual backbone of the atomic collision cascade. The tree indicates that the Ar atom plunges through the top half of the molecule without interacting strongly with the organic solid. At this stage, only one or two bond-scissions have occurred and the energy transferred to the medium is less than 50 eV. In the bottom half, the projectile undergoes a number of energetic collisions and generates a dense network of subcascades. All the energy of the projectile is transferred to the molecule and many carbon and hydrogen atoms are displaced from their initial position. Although the specifics of the trajectories may vary, Fig. 3(a) indicates a few common features of the collision cascade development in an organic solid:
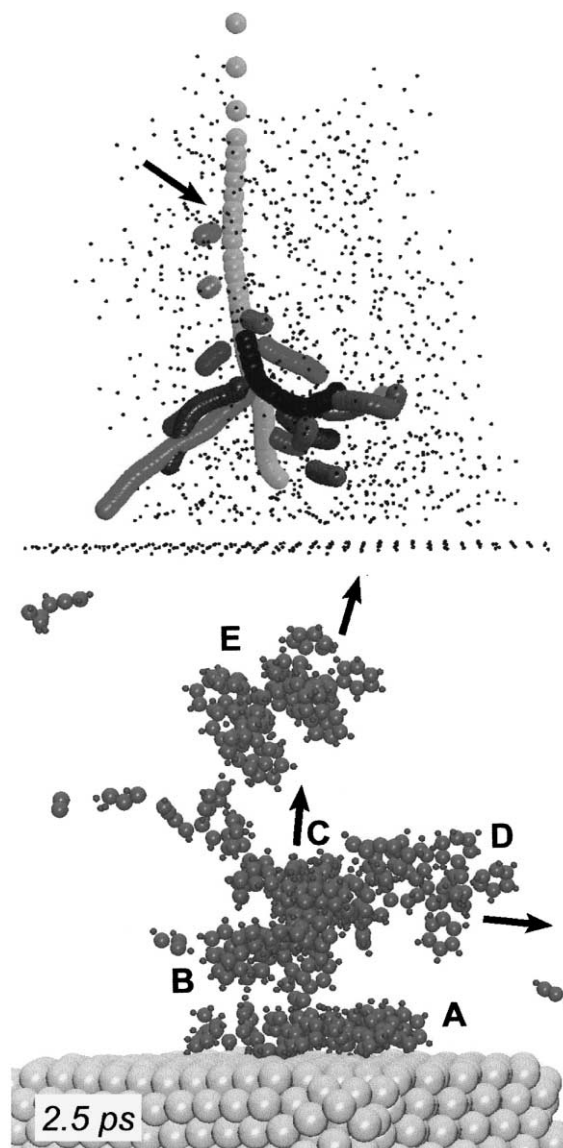
Fig. 3. (a) Collision tree of the first 100 fs of the interaction for a characteristic trajectory. The successive positions of the recoil atoms are indicated by large gray spheres provided that they are set in motion with more than 10 eV of energy. They are 'turned' off when their energy drops below 5 eV. (b) Movie snapshot of the MD simulation for the same trajectory after 2.5 ps. The labels indicate the different chain segments also described in Fig. 4. The arrows show the average direction of motion for the considered molecular segments.

- The slowing down of the projectile follows an almost straight path in the organic solid.

- The atomic subcascades are directed downwards or laterally, with no reflection towards the vacuum.
- The 500 eV Ar atom can dissipate his energy in the 25 Å thick organic layer.

The two first points contrast dramatically with results obtained for smaller molecules adsorbed on metal substrates, where the atomic cascade mainly occurs in the metal [10]. In that case, backscattering of the projectile and upward directed subcascades are frequent, directly inducing the ejection of secondary species in the first picosecond of the interaction. The third point is in agreement with TRIM calculations which indicate an average range of 31 Å for 500 eV Ar atoms bombarding a polystyrene layer under normal incidence [16].

The final result of the interaction is shown in the movie snapshot of Fig. 3(b), for the same trajectory. After 2.5 ps, several small fragments are moving upwards (C_6H_6) and laterally (C_2, C_2H_2, C_3H_3, C_3H_4) and a kilodalton chain segment ($C_{106}H_{106}$) is departing from the rest of the molecule with a total kinetic energy of 2.8 eV. The formation of the latter fragment has been triggered by the first bond-scission induced in the molecule by the projectile (arrow in Fig. 3(a)).

The link between the bond-scission induced during the atomic cascade stage (localized downward momentum) and the ejection of this 1592 Da chain segment (collective upward momentum) needs more explanation. It is analyzed in Section 3.3 of the article.

3.3. Molecular motion and chain segment emission

After a few hundreds of femtoseconds, the atomic collision cascade stage of the atom–organic solid interaction is over. The *average z*-velocities of the atoms in the molecule over the time range 0–500 fs provide an informative view of the collective processes involved after the atomic cascade development. In Fig. 4(a), the average *z*-velocities are plotted as a function of the atom index number in the molecule, atoms being labeled following the molecular backbone structure as a guideline. Because of the molecular arrangement, increasing numbers roughly correspond to an increasing
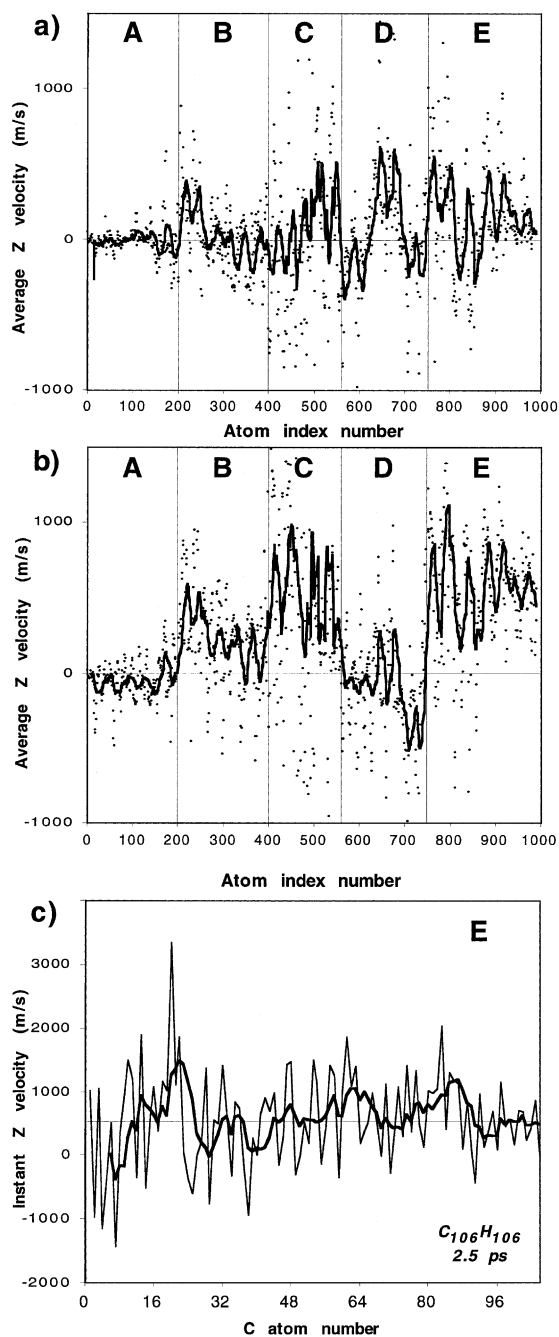
Fig. 4. Normal (*z*)-component of the velocity of the atoms for the trajectory described in Fig. 3. The full lines indicate the moving average of the data points, average *z*-velocity spectrum of the atoms over two time ranges: (a) 0–500 fs; (b) 500–1000 fs. Capital letters refer to the molecular chain segments labeled in Fig. 3. (c) Instant *z*-velocity spectrum of the C atoms belonging to the sputtered $C_{106}H_{106}$ fragment (E) at time $t = 2.5$ ps.

height of the atoms in the sample. The graph is divided in five parts labeled by capital letters (A–E), in reference to Fig. 3(b). Between 0 and 500 fs, a significant velocity (hundreds of m/s) is transferred to most of the atoms of the molecule, except for section A, which corresponds to carbon and hydrogen atoms lying at the interface with the silver substrate. The velocity spectrum roughly extends from -1000 to $+1000$ m/s. This wide overall variation and the fact that neighbor atoms can have very different velocities indicates that the nature of the excitation is vibrational (see hereafter). Nevertheless, the moving average of the data (black line) highlights a pattern in the velocities of neighboring groups of atoms. Indeed, each one of the full oscillations in Fig. 4(a) roughly encompasses two neighbor repeat units of the PS sample (32 atoms). In other words, if a local z-velocity maximum corresponds to an atom belonging to a given repeat unit, the next local minimum is found for the corresponding atom in the next repeat unit of the polymer. This pattern shows that beside high frequency vibrations at the atomic level, there is a sort of correlated motion within each repeat unit of the polymer, and this motion is oftentimes anticorrelated with that of the surrounding repeat units.

The average z-velocities have also been calculated for the time range 500–1000 fs (Fig. 4(b)). At that time, the average velocities of the different parts of the macromolecule (A–E) are clearly distinct, showing a certain correlation of the motion within the corresponding molecular segments. The direction of motion of these different segments, conserved over several picoseconds, is indicated by arrows in Fig. 3(b). Another important point is that the overall kinetic energy is significantly higher over this time range. This observation means that, whereas energy was mainly stored as potential energy in the first 500 fs, e.g. via the compression of the molecule, it is released as kinetic energy after 500 fs. Inside each chain segment, the velocity pattern corresponding to different repeat units is still present. The top of the molecule (part E) has a significant average upward velocity and it is on the verge of breaking free from the rest of the sample. It constitutes the $C_{106}H_{106}$ fragment identified above.

The *instant* z-velocities of the carbon atoms of the ejected $C_{106}H_{106}$ after 2.5 ps (Fig. 4(c)) show that the ejected chain segment keeps the memory of the vibrational excitation imparted to the molecule. This interpretation is suggested by the wide distribution of instant velocities (thousands of m/s) as compared to the center-of-mass z-velocity ($\sim$500 m/s) and by the fact that velocities are out-of-phase for neighbor carbon atoms. The out-of-phase motion of neighbor repeat units is somewhat damped but still present.

In summary, the atomic collision cascade energy dissipates in the organic solid over the first few hundreds of femtoseconds, inducing bond-scissions in the molecular backbone and creating ultimately vibrational excitation and collective motion at the molecular scale. The energy, predominantly stored as potential energy in the molecule, is transformed into kinetic energy of the atoms and molecular segments after 500 fs. Three different levels of motion are identified: interatomic vibration, correlated motion of the repeat unit of the polymer and correlated motion of larger chain segments. These collective uncorrelated and correlated motions lead to the swelling of the molecule and to the expansion of kilodalton chain segments in the vacuum.

4. Conclusion

MD simulations show that the bombardment of a large PS oligomer by a 500 eV Ar projectile induces an atomic collision cascade in the organic medium. Moving atoms collide with atoms at rest, creating bond-scissions and further sub-cascades. With time, the atomic cascade energy is transformed into a collective excitation of the atoms that leads to molecular motion and large kilodalton fragment ejection. This collective excitation appears to be partly uncorrelated, e.g. pure vibrational motion, and partly correlated, e.g. synchronized motion within chain segments.

From the methodological point of view, the comparison of polyatomic fragment nature and yields obtained with or without the use of long range forces shows that, even though long range forces provide a more accurate description of the

system, e.g. density and its dynamics, a model that neglects these forces still constitutes a reasonable approximation of the real system in the case of our polymer sample.

Our simulations provide new information about the emission of kilodalton fragments from large molecules such as polymers. Nevertheless, for direct comparison with experiment, the model could be refined by using higher projectile energies (5–25 keV), a set of various molecule configurations and an impact zone encompassing both the organic molecule and the silver substrate. To improve the understanding of organic solid sputtering, we also plan to investigate the emission of large organic molecules embedded in a low-molecular weight matrix (matrix-enhanced SIMS).

References

[1] P.A. Zimmerman, D.M. Hercules, A. Benninghoven, Anal. Chem. 65 (1993) 983.
[2] J.T. Mehl, D.M. Hercules, Macromolecules 34 (2001) 1845.
[3] B.J. Garrison, A. Delcorte, K.D. Krantzman, Account Chem. Res. 33 (2000) 69.
[4] K. Beardmore, R. Smith, Nucl. Instr. and Meth. B 102 (1995) 223.
[5] S.J. Stuart, A.B. Tutein, J.A. Harrison, J. Chem. Phys. 112 (2000) 6472.
[6] C.A. Daniels, Polymers: Structure and Properties, Technomic Publishing, Lancaster, Pennsylvania, 1989.
[7] D.E. Harrison Jr., CRC Crit. Rev. Solid State Mater. Sci. 14 (1988) S1.
[8] N. Winograd, B.J. Garrison, in: A.W. Czanderna, D.M. Hercules (Eds.), Ion Spectroscopies for Surface Analysis, Plenum Press, New York, 1991, p. 45.
[9] R. Chatterjee, Z. Postawa, N. Winograd, B.J. Garrison, J. Phys. Chem. B 103 (1999) 151.
[10] A. Delcorte, X. Vanden Eynde, P. Bertrand, J.C. Vickerman, B.J. Garrison, J. Phys. Chem. B 8104 (2000) 2673.
[11] D.W. Brenner, Phys. Rev. B 42 (1990) 9458.
[12] B.W. Schueler, Microsc. Microanal. Microstruct. 3 (1992) 119.
[13] A. Delcorte, X. Vanden Eynde, P. Bertrand, D.F. Reich, Int. J. Mass Spectrosc. 189 (1999) 133.
[14] A. Delcorte, P. Bertrand, B.J. Garrison, J. Phys. Chem. B 105 (2001) 9474.
[15] A. Delcorte, B.J. Garrison, J. Phys. Chem. B 104 (2000) 6785.
[16] J.P. Biersack, in: P. Mazzoldi, G.W. Arnold (Eds.), Ion Beam Modification of Insulators, Elsevier, Amsterdam, 1987, p. 26. Information concerning the program can be found at the following internet address: http://www.research.ibm.com/ionbeams/SRIM/.